

Berezinskii-Kosterlitz-Thouless-like localization-localization transitions in disordered two-dimensional quantized quadrupole insulators

C. Wang ^{1,*}, Wenxue He ^{1,2}, Hechen Ren,^{1,2,3} and X. R. Wang^{4,5}

¹Center for Joint Quantum Studies and Department of Physics, School of Science, Tianjin University, Tianjin 300350, China

²Tianjin Key Laboratory of Low Dimensional Materials Physics and Preparing Technology, School of Science, Tianjin University, Tianjin 300072, China

³Joint School of National University of Singapore and Tianjin University, International Campus of Tianjin University, Binhai New City, Fuzhou 350207, China

⁴Physics Department, The Hong Kong University of Science and Technology (HKUST), Clear Water Bay, Kowloon, Hong Kong
⁵HKUST Shenzhen Research Institute, Shenzhen 518057, China



(Received 14 June 2023; revised 12 December 2023; accepted 13 December 2023; published 10 January 2024)

Anderson localization transitions are usually referred to as disorder-driven quantum phase transitions from delocalized states to localized states. Here we report an unconventional “Anderson localization transition” in two-dimensional quantized quadrupole insulators. Such transitions are from symmetry-protected topological corner states to disorder-induced normal Anderson localized states, which can occur in the bulk as well as on the boundary. We show that these localization-localization transitions (transitions between two different types of localized states) can happen in both Hermitian and non-Hermitian quantized quadrupole insulators and investigate their criticality by finite-size scaling analysis of the corner density. The scaling analysis suggests that the correlation length of the phase transition, on the Anderson insulator side and near critical disorder W_c , diverges as $\xi(W) \propto \exp[\alpha/\sqrt{|W - W_c|}]$, a typical feature of Berezinskii-Kosterlitz-Thouless-like transitions.

DOI: [10.1103/PhysRevB.109.L020202](https://doi.org/10.1103/PhysRevB.109.L020202)

Introduction. Disorder-induced quantum phase transitions, known as Anderson localization transitions (ALTs) [1–4], are a fundamental topic in wave physics since disorders are ubiquitous in nature and profoundly affect the properties of states, as demonstrated in quantum Hall systems [3], topological Anderson insulators [5–7], and non-Hermitian systems [8–11]. The scope of ALTs is very broad, including metal-insulator transitions and quantum-Hall-plateau transitions that occur in topologically nontrivial systems [4]. They can be either second-order phase transitions between localized and extended states [12–15] or Berezinskii-Kosterlitz-Thouless (BKT) transitions between localized and critical states with fractal structures [16–20]. ALTs are generally considered as phase transitions from delocalized (extended or critical) states to localized states in disordered systems.

Here we report a disorder-induced phase transition from topologically nontrivial localized states to trivial localized states in two-dimensional quantized quadrupole insulators (2D QQIs) [21–25]. QQIs are 2D second-order topological insulators with in-gap zero-dimensional corner states characterized by a nonzero quadrupole moment. The second-order topological insulators survive at weak disorders, as genuine topological phases [26–29], in contrast to other localized states in deterministic fractals due to constructively interference [30]. Although Anderson localizations are surely dominant at strong disorders, how QQIs evolve into the

Anderson insulators (AIs) remains unresolved. Corner densities of wave functions show directly that QQIs transition to AIs as disorder increases, different from the delocalization-localization transitions reported in a second-order topological Anderson insulator [26]. The correlation lengths diverge exponentially on the AI side near the critical disorder, a feature reminiscent of BKT transitions [31,32].

The topological corner-dwelling states of QQIs have been observed in various materials, including sonic [33,34], photonic [35,36], cold atomic [37], and magnetic systems [38], whose Hamiltonians are non-Hermitian in principle. Therefore we consider a non-Hermitian Hamiltonian whose Hermitian part describes a QQI. Besides, in the presence of non-Hermiticity, such a model can support a transition from normal insulators in the Hermitian limit to non-Hermitian QQIs. Driven by disorder, both Hermitian and non-Hermitian QQIs undergo localization-localization transitions. Finite-size scaling analysis suggests that such transitions are BKT-like since the correlation lengths diverge as $\xi(W) \propto \exp[\alpha/\sqrt{|W - W_c|}]$, a behavior similar to the BKT-like criticality reported in other disordered systems [16–18].

Models. We consider a tight-binding model on a $L_x \times L_y$ square-octagon lattice subject to a non-Hermitian potential as shown in Figs. 1(a) and 1(b). The Hamiltonian reads

$$H = \sum_i c_i^\dagger \epsilon_i c_i + \left(\sum_{ij} c_i^\dagger \mathcal{T}_{ij} c_j + \text{H.c.} \right). \quad (1)$$

*Corresponding author: physcwang@tju.edu.cn

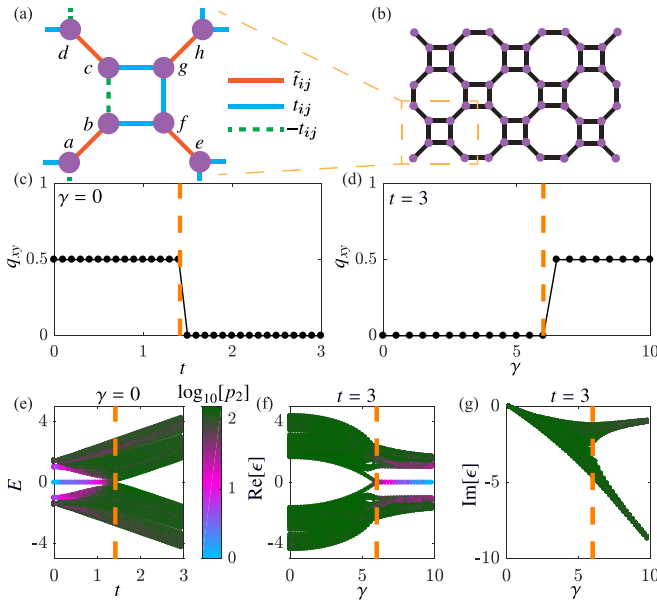


FIG. 1. (a) Unit cell of the square-octagon lattice. There are three different types of hopping, \tilde{t}_{ij} (orange), t_{ij} (blue), and $-t_{ij}$ (green), whose amplitudes are random. (b) A rectangular lattice of $L_x = 3$, $L_y = 2$ with lattice constant $a = 1$. (c) q_{xy} as a function of t for $\gamma = 0$ (Hermitian) and $W = 0$. (d) q_{xy} vs γ for $t = 3$ and $W = 0$. (e) Energy spectrum of $\gamma = 0$ for $L_x = L_y = 5$ in the clean limit. (f) and (g) $\text{Re}[\epsilon]$ and $\text{Im}[\epsilon]$ vs γ for $t = 3$ and $W = 0$. Colors in (e)–(g) map the common logarithm of participation numbers $\log_{10}[p_2(0)]$ interpreted later. Orange dashed lines in (c)–(g) separate QQIs and normal insulators.

Here, c_i^\dagger and c_i represent the creation and annihilation operators on site i . The nearest-neighbor hoppings \mathcal{T}_{ij} are \tilde{t}_{ij} , t_{ij} , and $-t_{ij}$ for the different types of hoppings shown in Fig. 1(a), where \tilde{t}_{ij} and t_{ij} distribute randomly and uniformly in the ranges $[(-W/2 + 1)\tilde{t}, (W/2 + 1)\tilde{t}]$ and $[(-W/2 + 1)t, (W/2 + 1)t]$, respectively. Hence W measures the degree of randomness. Non-Hermiticity is introduced by the on-site potentials with $\epsilon_i = i\gamma$ ($\gamma \in \mathbb{R}$) for the b, c, g , and f sublattices, and $\epsilon_i = 0$ otherwise. Below, we set $\tilde{t} = 1$ as the energy unit.

Topological invariance for clean QQIs. In the clean limit, the Bloch Hamiltonian of model (1) reads

$$h(\mathbf{k}) = \tilde{t}\tau_1 s_0 \sigma_0 + (i\gamma/2)\tau_0 s_0 \sigma_0 - (i\gamma/2)\tau_3 s_3 \sigma_0 \\ - [g_+(k_2)\tau_1 s_1 - g_-(k_2)\tau_2 s_2 + h(k_2)(\tau_2 s_1 + \tau_1 s_2)]\sigma_3 \\ + [g_+(k_1)\tau_0 s_0 + g_-(k_1)\tau_3 s_3]\sigma_1 + h(k_1)(\tau_0 s_0 + \tau_3 s_3)\sigma_2. \quad (2)$$

$\{\tau_{i=0,1,2,3}\}$, $\{s_{i=0,1,2,3}\}$, and $\{\sigma_{i=0,1,2,3}\}$ are unit and Pauli matrices on the sublattice spaces. $g_\pm(k) = (t/2)(\cos[k] \pm 1)$, and $h(k) = (t/2)\sin[k]$. Under certain conditions, $h(\mathbf{k})$ is a QOI for both Hermitian ($\gamma = 0$) and non-Hermitian ($\gamma \neq 0$) cases, where topologically protected states appear at the corners of a finite-size lattice such as that shown in Fig. 1(b).

Such corner states are featured by a bulk topological quadrupole moment q_{xy} , which can be calculated using nested Wilson loops [23]. A Wilson-loop operator in the x (y) direction is defined as \hat{W}_x (\hat{W}_y). In the Hermitian limit, the matrix elements of the Wilson-loop operator in the y direction

are given by a path integral over the first Brillouin zone (BZ), denoted by $\overline{\text{exp}}$,

$$[\hat{W}_y(k_1)]_{mn} = \overline{\text{exp}} \left[i \oint_{C_i} A_{mn}^y(k_1, k_2) dk_2 \right] \quad (3)$$

with C_i being a closed loop of $k_1 = q_i \Delta k_1$ and $k_2 = 0 \rightarrow \Delta k_2 \rightarrow 2\Delta k_2 \cdots \rightarrow (L_y - 1)\Delta k_2 \rightarrow 0$ and $\Delta k_1 = 2\pi/L_x$, $\Delta k_2 = 2\pi/L_y$. $A_{mn}^y(k_1, k_2) = i \langle u_m(\mathbf{k}) | \partial_{k_2} | u_n(\mathbf{k}) \rangle$ is the Berry connection, and $|u_n(\mathbf{k})\rangle$ is the occupied Bloch function [39,40]. By diagonalizing the Wilson-loop operator under periodic boundary conditions in both directions, one can define the Wannier Hamiltonian $\hat{\mathcal{H}}_y$ as $\hat{W}_y = e^{i\hat{\mathcal{H}}_y}$. We diagonalize the Wilson-loop operator $\hat{W}_y(k_1) |v_y^q(k_1)\rangle = e^{i2\pi v_y^q(k_1)} |v_y^q(k_1)\rangle$ and calculate the Wannier bands as $|w_y^q(\mathbf{k})\rangle = \sum_{n=1}^{N_{\text{occ}}} [v_y^q(k_1)]^n |u_n(\mathbf{k})\rangle$ with $[v_y^q(k_1)]^n$ being the n th component of the q th eigenket $|v_y^q(k_1)\rangle$. Here, N_{occ} is the number of occupied bands. The associated polarization in the subspace of Wannier bands is given by $p_x^q = -\frac{1}{2\pi} \int_{\text{BZ}} \tilde{A}_x^q(\mathbf{k}) d^2k$, where $\tilde{A}_x^q(\mathbf{k}) = i \langle w_y^q(\mathbf{k}) | \partial_{k_1} | w_y^q(\mathbf{k}) \rangle$ is the Berry connection defined in the Wannier bands. Likewise, one can define the polarization in the y direction by changing x into y (k_1 into k_2).

A nonzero polarization in the x (y) direction implies that the Wannier Hamiltonian $\hat{\mathcal{H}}_x$ ($\hat{\mathcal{H}}_y$) is a first-order topological insulator if the system is cut parallel to the x (y) direction. Naturally, the topological quadrupole moment is defined as $q_{xy} = 2p_x p_y$. A nonzero q_{xy} guarantees a second-order topological insulator with corner states, if open boundary conditions are applied in both directions. Here, $p_{x(y)} = \sum_q p_{x(y)}^q$. Figure 1(c) shows the numerically obtained q_{xy} as a function of t . It is seen that $q_{xy} = 0.5$ and 0 for $t < \sqrt{2}$ and $t > \sqrt{2}$. Hence a topological phase transition from QQIs to normal insulators happens at $t = \sqrt{2}$, where the bulk gap closes. This is further supported by the energy spectrum plot of model (1) on a square sample of $L_x = L_y = 5$; see Fig. 1(e).

Remarkably, non-Hermitian potentials can drive a quantum phase transition from normal insulators to QQIs, even when the system is topologically trivial in the Hermitian limit [41]. We generalize the Wilson-loop operators to non-Hermitian systems by rendering the Berry connection as $A_{mn}^{x(y)} = i \langle u_n^L(\mathbf{k}) | \partial_{k_1(k_2)} | u_m^R(\mathbf{k}) \rangle$ with $|u_m^R(\mathbf{k})\rangle$ and $|u_m^L(\mathbf{k})\rangle$ being the right and left Bloch kets, respectively, i.e., $h(\mathbf{k})|u_m^R(\mathbf{k})\rangle = \epsilon_m(\mathbf{k})|u_m^R(\mathbf{k})\rangle$, $h^\dagger(\mathbf{k})|u_m^L(\mathbf{k})\rangle = \epsilon_m^*(\mathbf{k})|u_m^L(\mathbf{k})\rangle$, and $\langle u_m^L(\mathbf{k}) | u_n^R(\mathbf{k}) \rangle = \delta_{mn}$ [42]. The numerically calculated q_{xy} as a function of γ for $t = 3$ is plotted in Fig. 1(d). Similar to the Hermitian cases, QQIs appear for $\gamma > 6$, which is also consistent with calculations of the complex energy spectrum of H ; see Figs. 1(f) and 1(g).

Hermitian systems. Having illustrated the existence of QQIs in the clean limit, we now investigate the disorder-induced quantum phase transitions. Consider Hermitian QQIs first. Model (1) preserves both time-reversal symmetry (TRS) and particle-hole symmetry (PHS) with symmetry operators $U_{\mathcal{T}} = \tau_0 s_0 \sigma_0 \otimes I$ and $U_{\mathcal{P}} = \tau_3 s_0 \sigma_3 \otimes I$, respectively. (Here, I is the unit matrix acting on the coordinate space.) Therefore model (1) of $\gamma = 0$ belongs to class BDI according to the Altland-Zirnbauer classification [43].

For $t < \sqrt{2}$ where $q_{xy} = 0.5$, we first compute the participation number $p_2(E) = \langle \sum_i |\psi_i(E)|^4 \rangle^{-1}$ for a state with

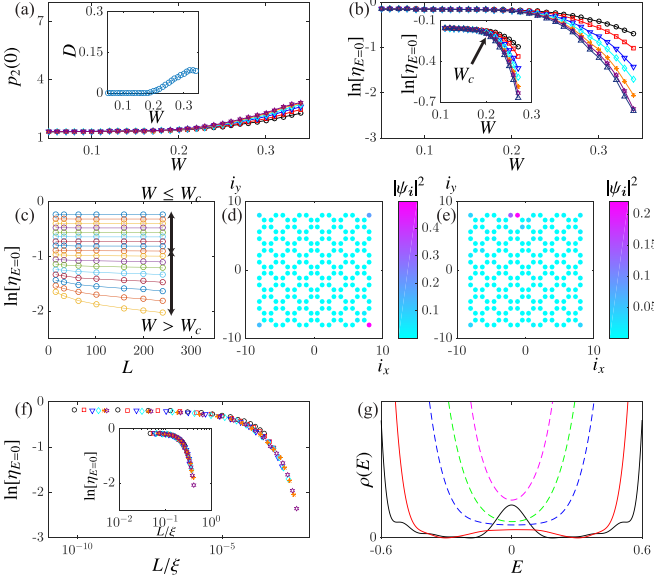


FIG. 2. (a) $p_2(0)$ as a function of W for the zero-energy state for $L = 15$ (black circles), 32 (red squares), 63 (blue inverted triangles), 101 (cyan diamonds), 159 (orange stars), and 200 (magenta hexagrams). Inset: wave-function dimension D as a function of W . (b) $\ln[\eta_{E=0}]$ as a function of W for $L = 15$ (black circles), 32 (red squares), 63 (blue inverted triangles), 101 (cyan diamonds), 159 (orange stars), 200 (magenta hexagrams), and 241 (dark blue upward pointing triangles). Inset: enlargement of (b) near W_c . The arrow locates the W_c obtained by the finite-size scaling analyses. (c) $\ln[\eta_{E=0}]$ as a function of various disorder strengths W . To have a better view, we shift each of the curves by -0.08 starting from $W = 0.11$. (d) Spatial distribution $|\psi_i|^2$ for $W = 0.05$ in a typical realization. $|\psi_i|^2$ for the four corners are marked. (e) Same as (d), but for $W = 0.35$. (f) Scaling function $\ln[\eta_{E=0}] = f(L/\xi)$ with $\xi \propto \exp[\alpha/\sqrt{|W - W_c|}]$. Inset: same as (f), but $\xi \propto |W - W_c|^{-\nu}$. (g) Average DOS $\rho(E)$ (arbitrary units) for $W = 0.02, 0.1, 0.2, 0.25, 0.3$. Those above (below) W_c are dashed (solid) curves.

energy E and amplitude $\psi_i(E)$, which measures how many sites the state effectively occupies [44–46]. It scales with the system size $L_x = L_y = L$ as $p_2 \propto L^D$ with $D = d$ (embedded spatial dimensionality), $D < d$, and $D = 0$ for extended, critical, and localized states, respectively [47].

Figure 2(a) exemplifies $p_2(0)$ as a function of W for $t = 0.5$ and L ranging from 15 to 200. It is seen that $p_2(0) < 3$ until $L = 200$. The dimension $D(W)$, obtained by a log-log plot of L and $p_2(0)$, is almost 0 [$D < 0.1$; see inset of Fig. 2(a)]. These features suggest that the zero-energy states are localized [48]. This is the main difference between our model and that of Ref. [26], where delocalized states appear near topological phase transition points, even though both belong to class BDI. Indeed, our numerical calculations are consistent with the one-parameter scaling theory of localization, which predicts that extended states are prohibited in the presence of TRS and spin-rotational symmetry ($U_{\mathcal{T}}^2 = I$) [49]. We further substantiate that all states of our model are localized by analyzing the dimensionless conductance obtained using the Landauer formalism [50] (see Supplemental Material Sec. S1 [51]).

As $p_2(0)$ is not a good scaling variable to identify the quantum phase transition in this system, we use the corner density $\eta_{E=0}(W, L) = \sum_{i \in \text{corners}} |\psi_i(0)|^2$, where the summation is over the four corner sites of Fig. 1(b) for given disorder W and size L . Since $\eta_{E=0}(W, L)$ describes the wave-function distribution of the zero-energy states on the corners, it should approach a finite nonzero constant for corner states and is zero for topologically trivial (both localized and extended) states. These features can be used to see whether a state with $E = 0$ is a corner state or not [27,28].

We calculate the ensemble-average $\ln[\eta_{E=0}(W, L)]$ for various W and L ranging from 15 to 241, as shown in Fig. 2(b) and its inset (enlargement near the critical disorder W_c). Clearly, there exists a critical disorder W_c separating two different regimes. (i) For $W < W_c$, $\ln[\eta_{E=0}] \simeq -0.15$, and $\partial \ln[\eta_{E=0}]/\partial L = 0$, indicating that the zero-energy states are corner states. (ii) For $W > W_c$, $\ln[\eta_{E=0}]$ decreases with L . This feature, together with the $p_2(0)$ results in Fig. 2(a), suggests that the zero-energy states are conventional localized states (at corners, edges, or bulk).

Such a transition from the QQIs to the AIs can also be seen by Fig. 2(c), where we plot $\ln[\eta_{E=0}]$ as a function of L for various W . We can see that below W_c the corner densities are size independent, while above W_c they decrease with size. Therefore Fig. 2(c) is an additional scaling argument to support the transition. Besides, the wave-function distributions for two typical disorders, $W = 0.05$ and $W = 0.35$, are plotted in Figs. 2(d) and 2(e), which are consistent with our analysis above.

We expect that $\ln[\eta_{E=0}]$ satisfies the finite-size scaling hypothesis [18]

$$\ln[\eta_{E=0}(W, L)] = f(L/\xi) + CL^{-y}, \quad (4)$$

where $\xi(W)$ is the correlation length, $f(x)$ is a scaling function, C is a constant, and $y > 0$ is the exponent for the irrelevant scaling variable. On the AI side, the correlation lengths can be treated as the localization lengths of localized states, like those for ALTs [2]. Differently, on the QQI side, the correlation lengths are infinite, i.e., $\xi = \infty$, such that the scaling function becomes $\ln[\eta_{E=0}] = f(0)$ for large sizes. This indicates that $\ln[\eta_{E=0}]$ is size independent for $W < W_c$, consistent with the numerical data shown in Fig. 2(b). Therefore we cannot properly define ξ on the QQI side.

To substantiate the single-parameter scaling hypothesis, we show in Fig. 2(f) and its inset that all curves of $\ln[\eta_{E=0}]$ on the AI side collapse into a single smooth curve $f(L/\xi)$ if proper ξ is chosen and the effect of irrelevant scaling variables is removed [20]. If ξ is assumed to follow a power-law divergence like conventional ALTs [3], $\xi \propto |W - W_c|^{-\nu}$, the critical exponent $\nu = 5.9 \pm 0.6$ is obtained. On the other hand, we can assume that such transitions are BKT-like with the correlation length ξ exponentially diverging as $\xi \propto \exp[\alpha/\sqrt{|W - W_c|}]$ and find a scaling function with $\alpha = 4.5 \pm 0.5$ and $W_c = 0.17 \pm 0.01$. This assumption can be supported by the existence of the disorder-driven BKT-like transitions in other systems [16–18].

To judge whether the transition is an ALT or is BKT-like, we calculate the goodness of fit through the χ^2 fittings for both exponential divergence $\xi \propto \exp[\alpha/\sqrt{|W - W_c|}]$ and

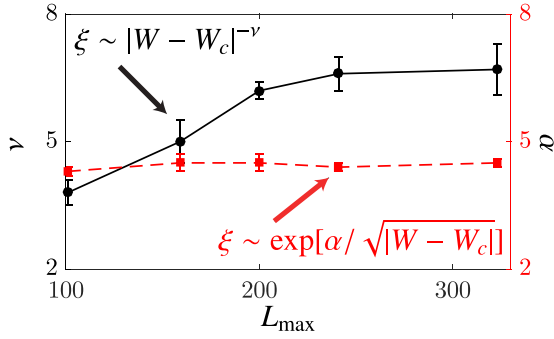


FIG. 3. Critical exponents of ν (power-law divergent assumption of ξ) and α (exponential divergent assumption of ξ) as a function of L_{\max} . The critical exponents are obtained using data for $L = 15, 32, \dots, L_{\max}$ with various L_{\max} .

power-law divergence $\xi \propto |W - W_c|^{-\nu}$. The former is $Q = 0.3$, far better than that of the power-law fit $Q = 4 \times 10^{-4}$, thereby supporting our claim pertaining to a BKT-like transition. In addition, we calculate the correlation lengths by χ^2 fitting of different system sizes. If the correlation lengths diverge in a power law like ALTs, the critical exponent ν should be size independent, as shown in Ref. [11]. However, we find that the obtained ν increases with size (see black curve in Fig. 3), such that our data do not support the power-law divergence assumption. On the other hand, if we assume an exponential divergence of ξ , the obtained α is size independent; see Fig. 3.

The origin of the quantum phase transition in Fig. 2(b) is revealed by the average density of states (DOS) plot, defined as $\rho(E) = \langle \sum_q \delta(E - E_q) \rangle / L^2$, as shown in Fig. 2(g). $\rho(E)$ is obtained from the kernel polynomial method [52]. The DOS is symmetric about $E = 0$ due to PHS. For $W < W_c$, we see

a gap in the bulk states near $E = 0$, which becomes smaller with the increase in W and disappears when $W > W_c$. The in-gap peak that stands for corner states also disappears when $W > W_c$. Hence this topologically quantum phase transition is a gap-closing transition, similar to those in three-dimensional second-order topological insulators [27] and Weyl semimetals [53].

Non-Hermitian systems. BKT-like transitions also appear in non-Hermitian QQIs. For $\gamma = 10$ and $t = 3$, model (1) is a non-Hermitian QOI with corner states at $\text{Re}[\epsilon] = 0$; see Fig. 1(f). Now, we generalize the participation numbers and the corner density by replacing $\psi_i(E = 0)$ by the right eigenfunction $\psi_i^R(\text{Re}[\epsilon] = 0)$.

Figure 4(a) and its inset display $p_2(0)$ and D as a function of W for $\gamma = 10$ and $t = 3$, from which one can see that all states are also localized. Model (1) with $\gamma \neq 0$ preserves TRS^\dagger , PHS^\dagger , and chiral symmetry with symmetry operators $U_{\mathcal{P}+} = \tau_0 s_0 \sigma_0 \otimes I$, $U_{\mathcal{T}-} = \tau_0 s_0 \sigma_3 \otimes I$, and $U_C = U_{\mathcal{P}+} U_{\mathcal{T}-}$ and belongs to class BDI^\dagger of the non-Hermitian Altland-Zirnbauer classification [54]. A theory proposed by Luo *et al.* predicts an equivalence of criticality between class BDI^\dagger and class AI in Hermitian systems [55], where all states are localized in 2D. Our calculations are consistent with this.

Although there is no delocalization-localization transition, a localization-localization transition from QQIs to AIs can be seen from the plot of $\ln[\eta_{\text{Re}[\epsilon]=0}]$, where $\partial \eta_{\text{Re}[\epsilon]=0} / \partial L = 0$ for $W \leq W_c = 0.08 \pm 0.01$ and $\partial \eta_{\text{Re}[\epsilon]=0} / \partial L < 0$ for $W > W_c$. One can choose a proper correlation length $\xi(W)$ such that $\ln[\eta_{\text{Re}[\epsilon]=0}]$ on the AI side merges into a single scaling function $f(x)$. The correlation length ξ diverges either in a power law $\xi \propto |W - W_c|^{-\nu}$ with $\nu = 7.61 \pm 0.02$ or an exponential decay $\xi \propto \exp[\alpha/\sqrt{|W - W_c|}]$ with $\alpha = 4.56 \pm 0.04$; see Fig. 4(c). Similar to the Hermitian cases, the goodness of fit Q for the fitting of $\xi \propto \exp[\alpha/\sqrt{|W - W_c|}]$ is 0.2, which is

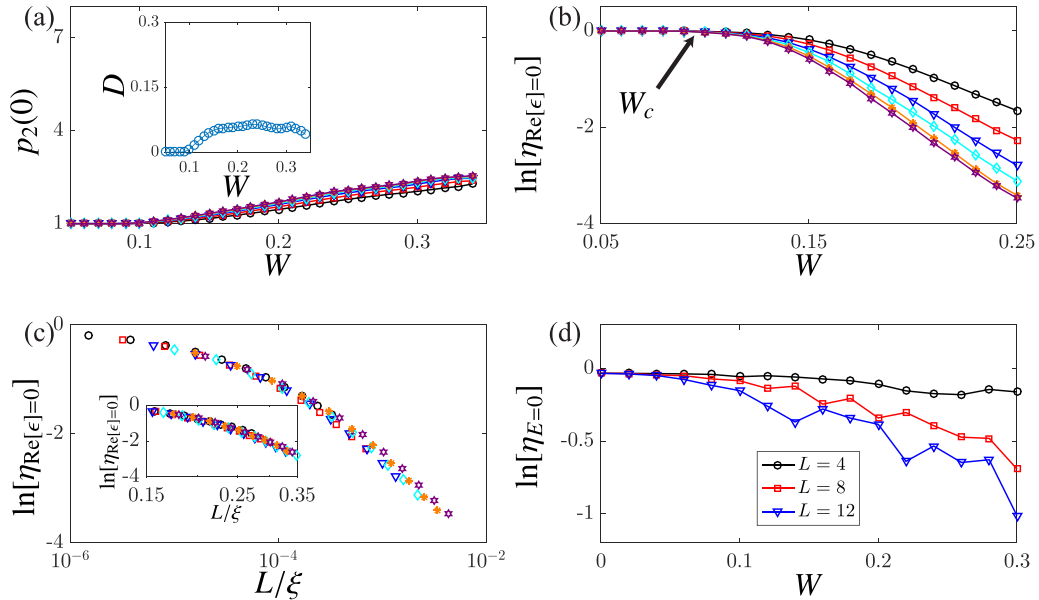


FIG. 4. (a) $p_2(0)$ as a function of W for the $\text{Re}[\epsilon] = 0$ state for $L = 15$ (black circles), 32 (red squares), 63 (blue inverted triangles), 101 (cyan diamonds), 159 (orange stars), and 200 (magenta hexagrams). Inset: $D(W)$ for $\text{Re}[\epsilon] = 0$. (b) $\ln[\eta_{\text{Re}[\epsilon]=0}]$ as a function of W for different L [same sizes as in (a)]. (c) Scaling function $\ln[\eta_{\text{Re}[\epsilon]=0}] = f(L/\xi)$ with $\xi \propto \exp[\alpha/\sqrt{|W - W_c|}]$ as (c), but for $\xi \propto |W - W_c|^{-\nu}$. (d) $\ln[\eta_{E=0}]$ data as a function of W from circuit simulation for $L = 4, 8, 12$. The system is a QOI when $W = 0$.

much larger than $Q = 10^{-4}$ for the fitting of $\xi \propto |W - W_c|^{-\nu}$. Since the goodness of fit for the power-law divergence is quite small and that for the exponential divergence is acceptable, we argue that the transition in Fig. 4(b) is BKT-like.

Experimental relevance. We design an LC circuit which is equivalent to model (1) in the Hermitian limit at resonance frequency (see Supplemental Material Sec. S2 [51]). The corner density is measurable: $\eta_{E=0}(W, L) = \sum_{i \in \text{corners}} |Z_i|/Z$ with Z_i and Z being the ground impedance of the four corner sites and the total impedance, respectively. We use LTSPICE [56], a well-established electric circuit simulator, to calculate $\ln[\eta_{E=0}]$ as a function of W for $L = 4, 8, 12$; see Fig. 4(d), which exhibits similar behaviors to those shown in Fig. 2(b) and serves as strong evidence for the localization-localization transitions.

Summary. In summary, we have shown that 2D QQIs, both Hermitian and non-Hermitian, can undergo disorder-driven localization-localization transitions, whose criticality is BKT-like. The BKT-like localization-localization transitions of corner states can also be seen in second-order topological insulators characterized by Z_3 Berry phases [25] (see Supplemental Material Sec. S3 [51]). Although our claim of BKT-like localization-localization transitions agrees with the field-theoretical approach on BDI class (same as our Hermitian QQIs) [57], whether the BKT-like transitions can happen for class BDI[†] (non-Hermitian QQIs) remains unclear.

Acknowledgments. This work is supported by the National Natural Science Foundation of China (Grants No. 12374122 and No. 11704061) and Hong Kong RGC (Grants No. 16300522, No. 16300523, and No. 16302321).

-
- [1] P. W. Anderson, Absence of diffusion in certain random lattices, *Phys. Rev.* **109**, 1492 (1958).
 - [2] B. Kramer and A. Mackinnon, Localization: theory and experiment, *Rep. Prog. Phys.* **56**, 1469 (1993).
 - [3] B. Huckestein, Scaling theory of the integer quantum Hall effect, *Rev. Mod. Phys.* **67**, 357 (1995).
 - [4] F. Evers and A. D. Mirlin, Anderson transitions, *Rev. Mod. Phys.* **80**, 1355 (2008).
 - [5] J. Li, R.-L. Chu, J. K. Jain, and S.-Q. Shen, Topological Anderson insulator, *Phys. Rev. Lett.* **102**, 136806 (2009).
 - [6] C. W. Groth, M. Wimmer, A. R. Akhmerov, J. Tworzydło, and C. W. J. Beenakker, Theory of the topological Anderson insulator, *Phys. Rev. Lett.* **103**, 196805 (2009).
 - [7] Y. Su, Y. Avishai, and X. R. Wang, Topological Anderson insulators in systems without time-reversal symmetry, *Phys. Rev. B* **93**, 214206 (2016).
 - [8] N. Hatano and D. R. Nelson, Localization transitions in non-Hermitian quantum mechanics, *Phys. Rev. Lett.* **77**, 570 (1996).
 - [9] Y. Huang and B. I. Shklovskii, Anderson transition in three-dimensional systems with non-Hermitian disorder, *Phys. Rev. B* **101**, 014204 (2020).
 - [10] X. Luo, T. Ohtsuki, and R. Shindou, Universality classes of the Anderson transitions driven by non-Hermitian disorder, *Phys. Rev. Lett.* **126**, 090402 (2021).
 - [11] C. Wang and X. R. Wang, Anderson localization transitions in disordered non-Hermitian systems with exceptional points, *Phys. Rev. B* **107**, 024202 (2023).
 - [12] S. N. Evangelou, Anderson transition, scaling, and level statistics in the presence of spin orbit coupling, *Phys. Rev. Lett.* **75**, 2550 (1995).
 - [13] Y. Asada, K. Slevin, and T. Ohtsuki, Anderson transition in two-dimensional systems with spin-orbit coupling, *Phys. Rev. Lett.* **89**, 256601 (2002).
 - [14] G. Orso, Anderson transition of cold atoms with synthetic spin-orbit coupling in two-dimensional speckle potentials, *Phys. Rev. Lett.* **118**, 105301 (2017).
 - [15] C. Wang and X. R. Wang, Anderson transition of two-dimensional spinful electrons in the Gaussian unitary ensemble, *Phys. Rev. B* **96**, 104204 (2017).
 - [16] X. C. Xie, X. R. Wang, and D. Z. Liu, Kosterlitz-Thouless-type metal-insulator transition of a 2D electron gas in a random magnetic field, *Phys. Rev. Lett.* **80**, 3563 (1998).
 - [17] Y.-Y. Zhang, J. Hu, B. A. Bernevig, X. R. Wang, X. C. Xie, and W. M. Liu, Localization and the Kosterlitz-Thouless transition in disordered graphene, *Phys. Rev. Lett.* **102**, 106401 (2009).
 - [18] C. Wang, Y. Su, Y. Avishai, Y. Meir, and X. R. Wang, Band of critical states in Anderson localization in a strong magnetic field with random spin-orbit scattering, *Phys. Rev. Lett.* **114**, 096803 (2015).
 - [19] C.-Z. Chen, H. Liu, and X. C. Xie, Effects of random domains on the zero Hall plateau in the quantum anomalous Hall effect, *Phys. Rev. Lett.* **122**, 026601 (2019).
 - [20] W. Chen, C. Wang, Q. Shi, Q. Li, and X. R. Wang, Metal to marginal-metal transition in two-dimensional ferromagnetic electron gases, *Phys. Rev. B* **100**, 214201 (2019).
 - [21] J. Langbehn, Y. Peng, L. Trifunovic, F. von Oppen, and P. W. Brouwer, Reflection-symmetric second-order topological insulators and superconductors, *Phys. Rev. Lett.* **119**, 246401 (2017).
 - [22] W. A. Benalcazar, B. A. Bernevig, and T. L. Hughes, Quantized electric multipole insulators, *Science* **357**, 61 (2017).
 - [23] W. A. Benalcazar, B. A. Bernevig, and T. L. Hughes, Electric multipole moments, topological multipole moment pumping, and chiral hinge states in crystalline insulators, *Phys. Rev. B* **96**, 245115 (2017).
 - [24] F. Schindler, A. M. Cook, M. G. Vergniory, Z. J. Wang, S. S. P. Parkin, B. A. Bernevig, and T. Neupert, Higher-order topological insulators, *Sci. Adv.* **4**, eaat0346 (2018).
 - [25] M. Ezawa, Higher-order topological insulators and semimetals on the breathing kagome and pyrochlore lattices, *Phys. Rev. Lett.* **120**, 026801 (2018).
 - [26] C.-A. Li, B. Fu, Z.-A. Hu, J. Li, and S.-Q. Shen, Topological phase transitions in disordered electric quadrupole insulators, *Phys. Rev. Lett.* **125**, 166801 (2020).
 - [27] C. Wang and X. R. Wang, Disorder-induced quantum phase transitions in three-dimensional second-order topological insulators, *Phys. Rev. Res.* **2**, 033521 (2020).

- [28] C. Wang and X. R. Wang, Robustness of helical hinge states of weak second-order topological insulators, *Phys. Rev. B* **103**, 115118 (2021).
- [29] H. Liu, J.-K. Zhou, B.-L. Wu, Z.-Q. Zhang, and H. Jiang, Real-space topological invariant and higher-order topological Anderson insulator in two-dimensional non-Hermitian systems, *Phys. Rev. B* **103**, 224203 (2021).
- [30] X. R. Wang, Magnetic-field effects on localization in a fractal lattice, *Phys. Rev. B* **53**, 12035 (1996).
- [31] V. L. Berezinskii, Destruction of long-range order in one-dimensional and two-dimensional systems having a continuous symmetry group I, Classical systems, *Sov. Phys. JETP* **32**, 493 (1971).
- [32] J. M. Kosterlitz and D. J. Thouless, Ordering, metastability and phase transitions in two-dimensional systems, *J. Phys. C: Solid State Phys.* **6**, 1181 (1973).
- [33] Z. Zhang, M. R. López, Y. Cheng, X. Liu, and J. Christensen, Non-Hermitian sonic second-order topological insulator, *Phys. Rev. Lett.* **122**, 195501 (2019).
- [34] H. Xue, Y. Ge, H.-X. Sun, Q. Wang, D. Jia, Y.-J. Guan, S.-Q. Yuan, Y. Chong, and B. Zhang, Observation of an acoustic octupole topological insulator, *Nat. Commun.* **11**, 2442 (2020).
- [35] K. Takata and M. Notomi, Photonic topological insulating phase induced solely by gain and loss, *Phys. Rev. Lett.* **121**, 213902 (2018).
- [36] B.-Y. Xie, G.-X. Su, H.-F. Wang, H. Su, X.-P. Shen, P. Zhan, M.-H. Lu, Z.-L. Wang, and Y.-F. Chen, Visualization of higher-order topological insulating phases in two-dimensional dielectric photonic crystals, *Phys. Rev. Lett.* **122**, 233903 (2019).
- [37] L. Li, C. H. Lee, and J. Gong, Topological switch for non-Hermitian skin effect in cold-atom systems with loss, *Phys. Rev. Lett.* **124**, 250402 (2020).
- [38] Z.-X. Li, Y. Cao, and P. Yan, Topological insulators and semimetals in classical magnetic systems, *Phys. Rep.* **915**, 1 (2021).
- [39] The numerical method in Ref. [40] is used to avoid the possible complication in gauge.
- [40] T. Fukui, Y. Hatsugai, and H. Suzuki, Chern numbers in discretized Brillouin zone: Efficient method of computing (spin) Hall conductances, *J. Phys. Soc. Jpn.* **74**, 1674 (2005).
- [41] Y. Tian, Z. Tan, W. Zhang, X. Han, and C. Cho, Analogous quadrupole topology induced by non-Hermiticity, *Phys. Rev. B* **107**, 094107 (2023).
- [42] X.-W. Luo and C. Zhang, Higher-order topological corner states induced by gain and loss, *Phys. Rev. Lett.* **123**, 073601 (2019).
- [43] A. Altland and M. R. Zirnbauer, Nonstandard symmetry classes in mesoscopic normal-superconducting hybrid structures, *Phys. Rev. B* **55**, 1142 (1997).
- [44] Numerically, we compute the participation numbers and the corner densities by using the KWANT package [45] and the SCIPY library [46] on PYTHON.
- [45] C. W. Groth, M. Wimmer, A. R. Akhmerov, and X. Waintal, Kwant: A software package for quantum transport, *New J. Phys.* **16**, 063065 (2014).
- [46] P. Virtanen, R. Gommers, T. E. Oliphant, M. Haberland, T. Reddy, D. Cournapeau, E. Burovski, P. Peterson, W. Weckesser, J. Bright, S. J. van der Walt, M. Brett, J. Wilson, K. J. Millman, N. Mayorov, A. R. J. Nelson, E. Jones, R. Kern, E. Larson, C. J. Carey *et al.*, SciPy 1.0: Fundamental algorithms for scientific computing in Python, *Nat. Methods* **17**, 261 (2020).
- [47] X. R. Wang, Y. Shapir, and M. Rubinstein, Analysis of multiscaling structure in diffusion-limited aggregation: A kinetic renormalization-group approach, *Phys. Rev. A* **39**, 5974 (1989).
- [48] Generally speaking, the wave function of a critical (extended) state occupies a fractal space of dimension $D \simeq 1.8$ ($D = 2$) in two dimensions. In our calculations, the dimensions of wave functions are very small, i.e., $D < 0.1$ for all W . We thus conclude that all $E = 0$ states of our model are localized. Indeed, we expect $D = 0$ for very large L ; see Refs. [18,20].
- [49] P. A. Lee and T. V. Ramakrishnan, Disordered electronic systems, *Rev. Mod. Phys.* **57**, 287 (1985).
- [50] A. MacKinnon, The calculation of transport properties and density of states of disordered solids, *Z. Phys. B* **59**, 385 (1985).
- [51] See Supplemental Material at <http://link.aps.org/supplemental/10.1103/PhysRevB.109.L020202> for a demonstration that the zero-energy states are always localized through the Landau formalism (Sec. S1), an illustration of an experimental scheme to observe the localization-localization transitions through electric circuits (Sec. S2), and proof that second-order topological insulators of a different type, featuring Z_3 Berry phases, also display BKT-like localization-localization transitions (Sec. S3).
- [52] A. Weiße, G. Wellein, A. Alvermann, and H. Fehske, The kernel polynomial method, *Rev. Mod. Phys.* **78**, 275 (2006).
- [53] S. Liu, T. Ohtsuki, and R. Shindou, Effect of disorder in a three-dimensional layered Chern insulator, *Phys. Rev. Lett.* **116**, 066401 (2016).
- [54] K. Kawabata, K. Shiozaki, M. Ueda, and M. Sato, Symmetry and topology in non-Hermitian physics, *Phys. Rev. X* **9**, 041015 (2019).
- [55] X. Luo, Z. Xiao, K. Kawabata, T. Ohtsuki, and R. Shindou, Unifying the Anderson transitions in Hermitian and non-Hermitian systems, *Phys. Rev. Res.* **4**, L022035 (2022).
- [56] <https://www.analog.com/en/design-center/design-tools-and-calculators/ltspice-simulator.html>.
- [57] E. J. König, P. M. Ostrovsky, I. V. Protopopov, and A. D. Mirlin, Metal-insulator transition in two-dimensional random fermion systems of chiral symmetry classes, *Phys. Rev. B* **85**, 195130 (2012).